 https://doi.org/10.3311/PPch.41234

Periodica Polytechnica Chemical Engineering, 69(3), pp. 480–492, 2025

Development and Characterization of Chitin-based Hydrogel Nanocomposites from Animal Shells for Sustainable Agriculture

Jamesraj Sathish[1], Ramasamy Palani[1*]

[1] Department of Chemical Engineering, Hindusthan College of Engineering and Technology, Coimbatore-641032, Tamil Nadu, India
[*] Corresponding author, e-mail: palani.chem@hicet.ac.in

Received: 11 June 2025, Accepted: 12 August 2025, Published online: 03 September 2025

Abstract

This paper presents a report on the design and performance testing of a nano-chitin-source-based hydrogel (*Portunus pelagicus* crab) shell-derived nano-hydrogel in support of sustainable agricultural uses in terms of its potential to be used in water retention and urea release. Using a multi-step acid hydrolysis method, nano-chitin could be extracted and introduced into a NaOH/urea aqueous solution whereby a hydrogel was formed. The prepared hydrogel was expected to minimize the loss of nutrients and increase the moisture holding capacity of soil in arid and semi-arid environments. The Fourier transform infra red spectra proved the existence of typical N-H and amide functional groups at 3257 cm^{-1} and 1631 cm^{-1}, respectively. In X-ray diffractograms crystalline peaks were observed at 9.35° and 23.2° which revealed that nano-chitin is partially de-crystallized after hydrogel formation. The scanning electon microscopic images exhibited about 55.5 nm wide semi-crystalline nanofibrilsand nanopores on the surface of the fibres favouring high water-retention capacity and nutrient loading capacity. Application of soil trials showed 50% higher water holding capacity and 88% urea release, which results in long-lasting nutrient. In a plant growth experiment using *Vigna radiata,* it was observed that plant seed germination and their initial growth are enhanced and therefore the gels are agronomically viable. Soil analysis of the soil before and after hydrogel addition showed that there was an improvement in the soil ammoniacal nitrogen and moisture content.

Keywords

chitin, nano-chitin, hydrogel, crab shells, gelatin, sustainable water

1 Introduction

The issues of climate change and constant shortage of freshwater have heavily affected the entire world of agriculture, making the search of possible solutions as much as important as increasing the efficiency of using resources and bringing crop yields to their enhancement. As the population all over the world is expected to surpass 9.7 billion people by 2050, there is a necessity to implement technologies that will improve the processes of retaining water in the soil and delivery nutrients to it without the expansion of environmental load [1]. Several materials have been explored to serve this purpose and include hydrogels-which are three-dimensional polymerization networks with the highasking abilities to hold water and release it slowly to the roots of plants [2, 3]. Hydrogels based on natural polymers, especially chitin-derived, have become an item of great interest have gained attention considering the fact that they are biodegradable, biocompatible and renewable [4]. The second most common biopolymer on earth is chitin, which is common in properties of crustacean shells, insect exoskeleton, and cell wall of the fungi [5]. Global chitin market, estimated having worth of 2.7 billion in 2022, is projected to experience a healthy 15.2% compound annual growth rate between 2023 and 2030, due to its viability in various fields, such as agriculture, biomedicine, and environment remediation [6, 7].

Chitin in the nano window which is obtained by reducing bulk chitin to the nano scale has a larger surface area, mechanical strength and reactivity than microstructured chitin [8]. Such properties contribute greatly to the hydrogel performance in the water retention and its structural capability. As an intelligent delivery system of nutrients, nano-chitin-based hydrogels can be used in agriculture as per the premises of precision farming and Agriculture 4.0 [9, 10]. These systems have the potential to halve the needs of taking up irrigation and at the same time increase the nutrient

Cite this article as: Sathish, J., Palani, R. "Development and Characterization of Chitin-based Hydrogel Nanocomposites from Animal Shells for Sustainable Agriculture", Periodica Polytechnica Chemical Engineering, 69(3), pp. 480–492, 2025. https://doi.org/10.3311/PPch.41234

use efficiency [11]. With a market valuation of USD 2.4 billion in 2024, the global market of controlled-release fertilizers is expected to reach USD 3.2 billion by 2029 [12]. Leaching and volatilization loss of traditional fertilizers is common and the ratio of the fertilizer to that taken up by crops is 30 to 50 and 10 to 45% of nitrogen and phosphorus, respectively [13]. These losses can be reduced through using hydrogels enriched with nano-chitin to provide a maintaining release of nutrients in addition to improvement in soil structure and moisture [14–17]. In the past, it has been demonstrated that nano-chitin hydrogels were able to provide swelling capacities over 540% and an increased seed germination of 15 to 20% during drought conditions [18–25]. The comparative Table 1 in this paper gives an overview of the different studies that have evaluated chitin based hydrogels indicating their different performance [26]. Nevertheless, a number of issues are not covered by the current studies. Among them are insufficient large-scale synthesis approaches to nano-chitin hydrogels, unappy correlation between performance under ideal conditions and those applied in the real soil environment, and minimal research performed to assess water retention and nutrient release kinetics within a single framework [27–29].

Moreover, further research is required to assess the environmental fate of residue of nanoparticles as well as reproducibility of the structural and functional characteristics. In this paper, the researcher tends to these limits by creating an agricultural-optimized nano-chitin-based hydrogel of the crab shell waste. The synthesized hydrogel was investigated into its chemical framework, as well as its morphology via Fourier transform infrared spectoscopy (FTIR), and X-ray diffraction (XRD) and scanning electon microscopy (SEM) evaluations. Its performance was tested with respect to functional features by carrying out the release study in urea, water retention test, soil parameter survey, and plant development trial, with the help of *Vigna radiata* vegetable crop. Water holding capacity of the hydrogel was increased by 50% and nutrient release efficiency of the hydrogel was 88%, which means that a sustainable way of managing crops through a scalable, biodegradable solution has been found. Overall, we have given a prospective solution of the problem of resource-friendly agriculture in this work, bringing together these two properties of nano-chitin: structural benefits and a hydrogel carrier optimized to support controlled release and controlled moisture retention. The results lead to the progress of the smart input of bio-based agriculture and circular material processing in line with sustainable development objectives.

2 Materials and methods

2.1 Materials

The materials used for chitin preparation made up of *Portunus pelagicus* crab shell, sodium hydroxide, hydrochloric acid and distilled water. For the preparation of nano-chitin, the following chemicals were employed: sodium acetate, glacial acetic acid, potassium hydroxide sodium chlorite, sodium chloride, and sodium azide. In the process of hydrogel preparation, the key materials comprised nano-chitin, urea and sodium hydroxide all of analytical grade and purchased from Sigma Aldrich [29]. By employing these meticulously selected materials, the hydrogel formulation

Table 1 Comparison of chitin-based hydrogels with respect to water holding and nutrient release efficiencies

Material name	Water holding capacity (%)	Nutrient release efficiency (%)	Biodegradability (days)	Other metrics	Reference
Chitosan-based superabsorbent hydrogel	27	72	15	Tensile strength: 0.54 MPa; Elongation at break: 2203.7%; Good mechanical strength.	[14]
Starch-based biodegradable superabsorbent hydrogel	30	76	15	Medium mechanical strength within high swelling capacity 380-490% reported at pH 9.4.	[15]
Nanochitin hydrogels	39	82	15	High mechanical strength and swelling capacity; swelling capacity reported at 545.81% at pH 7.5 and tunable mechanical properties.	[16]
Nanocellulose/wood ash-reinforced starch–chitosan hydrogel	20	65	15	Swelling capacity: 200-420% in distilled water and 104-220% in saline medium; Enhanced mechanical properties due to incorporation of nanocellulose and wood ash.	[26]

achieved enhanced water retention and controlled release of fertilizer, as demonstrated through rigorous experimental analysis and structural characterization.

2.2 Experimental

2.2.1 Chitin preparation

A total of 1500 g of the crab shells were cleaned, dried and ground to powder. Out of this 1200 g of the prepared powder was employed in the extraction of chitin. Demineralization of the crab shell powder was executed by adding 100 mL of a 7% HCl solution to remove calcium carbonate and calcium phosphate minerals. The crab shell powder was gradually added to the HCl solution while stirring and heating continuously at 60-70 °C [30]. Then, it was allowed to settle under gravity to remove mainly calcium carbonate minerals. Next, deproteinization was performed by adding 50 mL of a 20% NaOH solution at 60-70 °C with constant stirring to the demineralized crab shell powder. This process decomposed the albumen into water-soluble amino acids. The mixture was then filtered and dried in an oven at 80 °C for 2 h to obtain chitin as shown in Fig. 1.

2.2.2 Nano-chitin preparation

1000 g of the above processed chitin was taken to prepare nano-chitin by suspended in a 5 wt% KOH solution and heated up to temperature of 60-70 °C for 6 h, then kept overnight at room temperature with continuous stirring, filtered, and rinsed with distilled water to remove protein impurities [31]. The resulting material underwent a bleaching process in a solution containing $NaOCl_2$ and sodium acetate buffer at pH 4.0 at 80 °C for 6 h, with solution replacement every 2 h followed by rinsing. The only reason why sodium azide was added to the chitin suspension was as an antimicrobial agent so as to eliminate microbial growth during storage. Before the formation of hydrogel, the suspension was duly washed to remove the remaining sodium azide, thus making sure that none of it remained in the end hydrogel. Subsequently, the material was soaked in a 5 wt% KOH solution for 48 h, followed by centrifugation and hydrolysis using 3 M HCl at boiling temperature for 90 min with stirring. The dispersion underwent dilution, ultrasonic treatment for proper dispersion, and addition of sodium azide before storage as shown in Fig. 2.

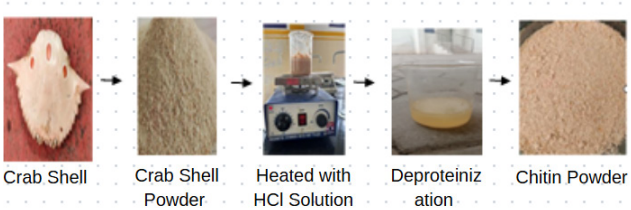

Fig. 1 Chitin preparation process

2.2.3 Hydrogel preparation

800 g nano-chitin powder was dispersed in an 8 wt% NaOH/4 wt% urea aqueous solution. The mixture was maintained at −20 °C while agitated twice within 36 h. After centrifugation to yield a 637 g chitin was obtained. The absence of precipitate in the supernatant indicated total dissolution. The undissolved mass was then separated, dried, and weighed. The solubility was calculated as:

$$\text{Solubility}(\%) = \left(\frac{W_o - W_r}{W_o}\right) \times 100\,, \tag{1}$$

where, W_o = initial mass of the nano-chitin (800 g) and W_r = mass of undissolved residue after centrifugation (637 g).

The analysis demonstrated 79.6% dissolution, confirming that nano-chitin was mainly solubilized in the NaOH/urea system and validating its use for in hydrogel formation. Due to the numerous junction points between nano-chitin chains the nano-chitin hydrogel was formed when the temperature reached 30 °C. It was facilitated by the exposed hydroxyl groups of the nano-chitin contributing to the spontaneous self-association and forming a cross-linked network structure as shown in Fig. 3.

The release behaviour of the nano-chitin hydrogel was evaluated by incorporating 5 wt% urea at the time of hydrogel formation. The release experiment was established using a static water dissolution method. 1 g of dry hydrogel was immersed in 100 mL distilled water at room

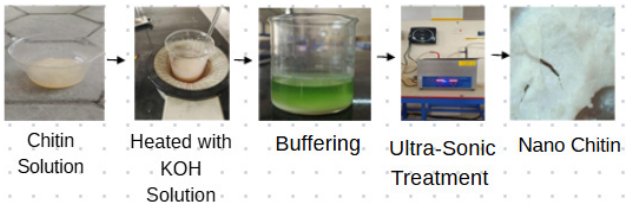

Fig. 2 Nano-chitin preparation process

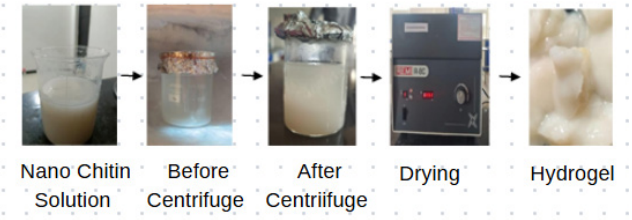

Fig. 3 Hydrogel preparation process

temperature. The urea content was determined at predetermined times in the extraction solution with a UV-Vis spectrophotometer (Prolab India, Mumbai, India) at 278 nm and the cumulative release of urea was calculated. The kinetics of urea release were fitted to the Higuchi model, which describes a diffusion-controlled release mechanism.

2.2.4 Soil test parameters

A baseline understanding of the current characteristics of the soil, including pH, nitrogen level, organic matter content, and microbial activity, were obtained through soil testing prior to hydrogel application. These data are essential for assessing how the hydrogel affects soil health.

Determining the chemical, physical, and biological characteristics of soil was done through soil testing. It is employed to ascertain whether the soil is suitable for various agricultural uses, including the cultivation of crops or the production of food. When irrigation facilities are available, the unique properties of the hydrogel can help alleviate the moisture stress of the crop plant by retaining water and nutrients from their surroundings. This technology may also reduce the amount of irrigation that crops require. From sampling to analysis and interpretation, the experimental process for handling soil testing entails a number of procedures that guarantee accurate data for solid decisions. The collection of representative soil samples, their appropriate preparation and storage, laboratory testing for certain parameters, and interpretation of the results in light of the particular crop and soil conditions are all crucial procedures. When hydrogels are wet, their high water content usually makes them malleable and squishy, frequently giving them a jelly-like quality. It is possible to incorporate the hydrogel into the soil by first soaking it and then combining it with the soil. Larger regions are appropriate for the dry technique. The soil test parameters were determined three times to have a correct result before the hydrogel inserted in the agricultural plot and the results are given on Table 2 [32–52].

3 Results and discussions

3.1 FTIR of crab shell powder

FTIR technique was employed to assess the degree of deacetylation (DA) and to characterize the functional groups present (Bruker, Karpagam University Research Lab (P-Lab, Coimbatore, India)). Evidently, FTIR spectra confirmed the presence of C=O and Ca−O group bonds, which are indicative of calcium carbonate. The peaks in the FTIR spectrum can be used to characterize calcium carbonate molecules. FTIR and XRD analyses were performed thrice in order to ensure reproducibility of the spectra. The results of the FTIR spectrum analysis verified that the materials were chitin and chitosan by displaying functional groups in various bands. The spectral vibrations of the functional groups in crab shell powder preparations were examined through FTIR, covering the wavelength range of 4000-450 cm^{-1} with a resolution of 4 cm^{-1}. The absorption peaks at 1020 cm^{-1} and 1071 cm^{-1} confirm the presence of C−O stretching and C−O−C bond, the peak at 1153 cm^{-1} is assigned to asymmetric bridge oxygen stretching as shown in Fig. 4.

The FTIR spectra display the distinctive calcite peaks at 1311 cm^{-1} and 1375 cm^{-1}, which are derived from the stretching vibrations of the carbonate ions brought by the existence of the asymmetrical CO_3^{2-} ions. Because of their vibrational mode, carbonate ions are discovered to occupy two distinct locations in carbonate apatite peaks. Significant peaks are also seen at 1556 cm^{-1} and 1622 cm^{-1}. The aforementioned distinctive peaks are caused by hydrogen bonding and correlate to the vibration of hydroxyl groups and N−H bond vibrations in $-NH_2$ primary amine groups. The absorption peak observed at 1622 cm^{-1} corresponds to the amide I band, which arises primarily from the C=O stretching vibration of the secondary amide group. In addition, a broad absorption band detected at 3255 cm^{-1} can be attributed to the N–H stretching vibration, which is often broadened due to hydrogen bonding interactions [53].

The DA, an important factor in characterizing chitin and chitosan, was calculated from the intensity ratios of the characteristic FTIR peaks, following the established FTIR absorbance ratio method.

$$\mathrm{DA}(\%) = \left(\frac{A_{1655}}{A_{3450}}\right) \times 100\,, \tag{2}$$

where A_{1655} is the absorbance of the amide I band (C=O stretch) and A_{3450} is the absorbance of the OH stretching band with wavenumber of 3450 cm^{-1}.

Similarly, the molecular mass (M) of chitosan was calculated by using the Mark–Houwink equation (Eq. (3)) [54–56]. The Mark-Houwink equation relates M with intrinsic viscosity and contributes to the assessment of the physicochemical properties necessary for useful application.

$$[\eta] = K \times M^{\alpha}\,, \tag{3}$$

where [η] is intrinsic viscosity, K and α are system constants [Table 3].

The stretching band of N−H was found distinct at 3256 cm^{-1}. The aliphatic −OH and −NH stretching vibrations of the free amino groups are represented by the

Table 2 Initial soil test parameters before hydrogel application

S. No.	Parameters	Unit	Test method	Results
1	Water content	%	IS 2720-2 [32]	8.86
2	Organic matter	%	IS 2720-22 [33]	0.78
3	pH value	-	IS 2720-26 [34]	8.36
4	Specific electrical conductivity	µs/cm	IS 14767 [35]	480
5	Sulphate	mg/100 g	SOP No. Soil/010 [36]	48
6	Available phosphorous	µg/g	SOP No. Soil/001 [37]	35
7	Soluble calcium and magnesium	meq/L (milliequivalents per liter)	SOP No. Soil/009 [38]	1.22
8	Soluble calcium	meq/L	SOP No. Soil/008 [39]	1.22
9	Carbonate	meq/L	SOP No. Soil/005 [40]	Nil
10	Bicarbonate	meq/L	SOP No. Soil/003 [41]	0.18
11	Chloride	meq/L	SOP No. Soil/006 [42]	22.1
12	Bulk density	g/mL	SOP No. Soil/004 [43]	1.35
13	Pore space	%	SOP No. Soil/007 [44]	26
14	Ammoniacal nitrogen	mg/kg	IS 14684:1999 [45]	Below detectable limit (BDL) (Detectable limit (DL): 1.0)
15	Total Kjeldahl nitrogen	%	IS 14684:1999 [45]	0.0388
16	Water holding capacity	%	SOP No. Soil/011 [46]	50
17	Soluble magnesium	meq/L	SOP No. Soil/009 [38]	BDL(DL: 0.2)
18	Soil texture	-	FAO method [47]	Silty loam
19	Sand	%	Robinson pipette method [48]	17.5
20	Silt	%		72.8
21	Clay	%		9.7
22	Chemical oxygen demand	mg/kg	Inhouse method [49]	13447
23	Biochemical oxygen demand	mg/kg	FAO method [50]	1450
24	Soluble sodium	mg/kg	FAO method [51]	1025
25	Soluble potassium	mg/kg	FAO method [52]	88
26	Cation exchange capacity	meq/100 g	FAO method [52]	16.5

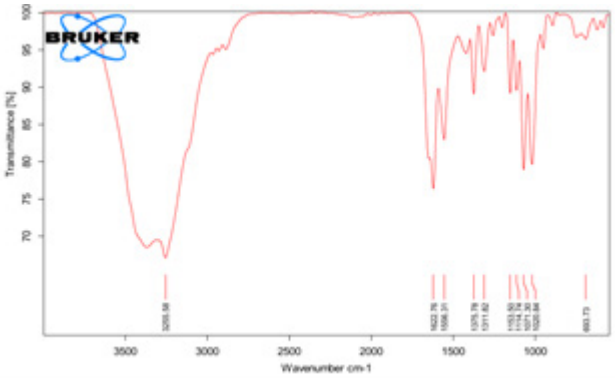

Fig. 4 FTIR spectrum of crab shell powder

absorption peaks seen in at 3256 cm^{-1} for the extracted crab chitosan. The distinctive phosphate stretching vibration band appears at 1020 cm^{-1}. The absorption band at 693 cm^{-1} is due to N–H bending vibrations.

Table 3 Molecular mass calculation on different intrinsic viscosity

Intrinsic viscosity (dL g^{-1})	Molecular mass (g mol^{-1})
0.20	8.6×10^3
0.40	2.1×10^4
0.60	3.4×10^4
0.80	4.9×10^4
$K = 1.57 \times 10^{-4}$ dL g^{-1}; $\alpha = 0.79$	

3.2 FTIR of nano-chitin powder

In addition to the rapidly evolving field of nanotechnology that deals with the properties of materials in the range of 1-100 nm, nano-chitin powders were prepared and studied by FTIR spectroscopy (Fig. 5). This material is applied more recently worldwide due to its biodegradable nature, size of 10-20 nm and large surface-to-mass ratio. All the

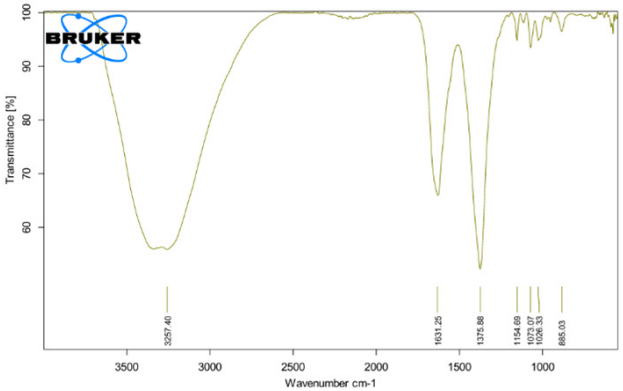

Fig. 5 FTIR spectrum of the nano-chitin powder

nano-chitin powders spectra revealed that their spectral characteristics closely match those of commercial chitin. The spectral vibrations of the functional groups in chitin preparations were examined with FTIR, covering the wavelength range 4000-450 cm^{-1} with a resolution of 4 cm^{-1}. The band at 1073 cm^{-1} confirms the presence of C−O stretching and C−O−C bond, the band at 1154 cm^{-1} is assigned to asymmetric bridge oxygen stretching. The band is linked to CH_2 bending vibrations and CH_3 symmetric deformation modes related to $CaCO_3$. The band at 1631.25 cm^{-1} is assigned to the amide II band (NH) stretching amide I (C=O) secondary amide, the band at 3256 cm^{-1} corresponds to the bending of N-H stretching.

The peak detected at 885 cm^{-1} corresponds to the ring stretching of chitin, the peak observed at 1026 cm^{-1} and the region 1026 to 1154 cm^{-1} contains the distinctive shoulder bands resulting from the chitin shell and protein contents. The band peaking at 1631 cm^{-1} corresponds to the C−H stretching band, while the wide band of N-H stretching band is located at 3257 cm^{-1}. It is challenging to distinguish the odd dominating bands of proteins and chitin at 1073 and 1154 cm^{-1}, because they strongly overlap with the bands originating from the bulk $CaCO_3$ phase in the range 885 to 1026 cm^{-1}. It is evident from the lack of a peak at 1556 cm^{-1} that the chitin is pure and free of protein contaminants. Because of the existence of aldehydic bonds, the spectra of nano-chitin and chemically crosslinked nano-chitin showed a new peak at 1631 cm^{-1}. It is evident from significant peaks for imine bonds at 3257 cm^{-1} that the chemical cross-linking between the chitin nanofibrils was successful.

The FTIR spectral comparison indicates that nano-chitin has sharper amide and hydroxyl peaks without the presence of bands corresponding to proteins, indicating higher purity and successful nano-conversion.

3.3 XRD of nano-chitin and hydrogel

To ascertain the crystal-like nature, XRD was utilized (Shimadzu XRD-6000 X-Ray Diffractometer, Karunya University (Safire Scientific)). It is an effective method for determining the physical characteristics, chemical composition and crystallographic structure of nano-chitin. Compared to chitosan, which typically exhibits broad, diffuse and less dominant peaks, nano-chitin exhibits well-resolved, intense peaks, indicating that chitin is more crystalline than the chitosan. From the XRD pattern it clearly shows that it is a well-ordered crystalline material. The position of the peaks in the XRD corresponds to the interatomic spacing within the crystal lattice and it is represented as 2θ where θ is the diffraction angle. The scattering strength is found to be influenced by the number of atoms contributing to the diffraction. As a result the intensity of the peak increases to considerably signifying the preferred orientation of the crystal and the porosity of the material is low. The stronger peak intensity in the diffraction pattern shows a clear preferred crystallographic orientation. At the same time, it suggests less porosity in the material.

The architectures of the wet gel and nano-chitin samples differ greatly, as demonstrated by the diffraction patterns. The diffraction pattern of the gel (which was dried in vacuum oven) without conditioning in water shows a maximum at $2\theta \approx 5$ seen in Figs. 6 and 7. After brief conditioning periods (3 to 6 h), this peak is barely discernible. After the sample has been conditioned in water for 24 h, it is clear. All the diffraction patterns show a broad halo at $2\theta = 11°$. The characteristic maximum for chitosan at $2\theta \approx 20°$ shows a notable variation. For gels that have been conditioned in water, this maximum is more noticeable.

In the XRD patterns of the sample A two broad crystalline reflections at 9.3° and 23.3° are evident within the 2θ range 5-45°, indicating the presence of chitin in sample A. Sample B exhibits three crystalline reflections at 9.3°, 23.3° and 27.2° within the same 2θ range. Notably, the crystalline reflections at 9.3° and 23.3° are noticeably reduced compared to those observed in sample A, implying a decrease in nano-chitin crystallinity during the dissolution and regeneration process. However, the crystalline reflection at 27.2° increases due to the alkaline deacetylation, consistent with the findings in literature [57]. The average crystallite size D of the nano-chitin was calculated from the Debye–Scherrer formula:

$$D = \frac{K\lambda}{\beta \cos\theta}, \tag{4}$$

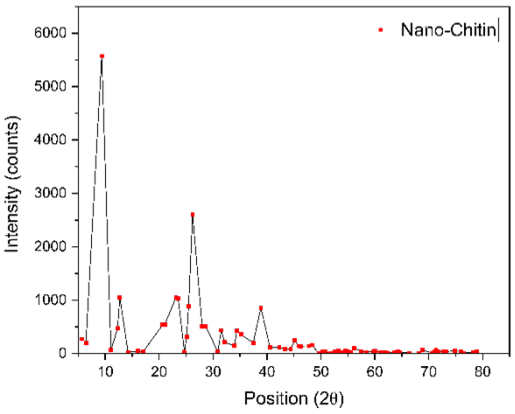

Fig. 6 XRD diffractogram of nano-chitin (red dot: position of 2θ (nano-chitin); black line: diffractogram)

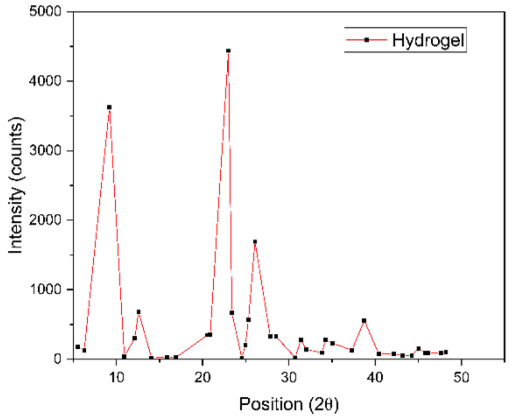

Fig. 7 XRD diffractogram of the hydrogel

where D is the crystallite size, K is the shape factor (0.9), λ is the X-ray wavelength (0.15406 nm), β is the full width at half maximum (FWHM) in radian, and θ is the Bragg angle.

According to the largest peak at $2\theta \approx 23.3°$, the average crystallite size was then determined as about 14.8 nm, which confirms the nanostructure nature of the fabricated chitin. The given parameter offers more proof that the material has a crystalline structure and specific nanostructural features.

The deacetylation of crab shell nano-chitin was carried out by maintaining the crystalline properties of nano-chitin. From the data it is clear that the deacetylation occurred on the surface and the interior was found to be unaltered, indicating that the physiochemical properties of the nano-chitin were controlled by the deacetylation reaction. The XRD pattern proves that the structure of the nano-chitin and hydrogel samples differ significantly. Within the 2θ range 5-45 the peak is hardly visible in the diffractogram of hydrogels indicating that the sample conditioning causes a remarkable change in the hydrogel. It is also found that it is enhancing for gels conditioned in water. Compared to nano-chitin, the XRD pattern of the hydrogel exhibited broader and weaker peaks, confirming that the crystallinity is lower due to the partiel formation of a polymer network and hydration.

Swelling degree tests were performed by immersing dried samples into deionized water and a 1% urea solution, respectively, at room temperature. Comparing the levels of swelling, nano-chitin hydrogel swelled more in urea than in water, demonstrating its good fertilizer retaining potential.

3.4 SEM analysis of nano-chitin

SEM uses the focused electron beam for surface imaging for structural and morphological evaluation (ZEISS, Super scientific). SEM helps in elucidating the existence of pores, certain contaminants and morphological alterations. The particle size and structural characteristics can be explained using SEM. A double-sided carbon tape was used to mount the powdered sample. SEM gives precise details about the size and shape of the nano-chitin surface. A working distance of 9.5 mm and an accelerating voltage of 10.0 kV were used to record SEM pictures. Prior to imaging, the nano-chitin suspension was dried at 400 °C for 30 min. Every other sample was vacuum-dried for at least 48 h. The various drying techniques were employed to attain varying degrees of crystallinity or to investigate how the various drying conditions affected the structure or characteristics of the final nano-chitin. By comparing the resultant chitin samples, we can comprehend how the drying circumstances affect the mechanical strength and solubility of the final products, among other characteristics. Vacuum drying may preserve the chitin structure whereas high-temperature drying may cause alterations. Agglomeration should be reduced. It makes it hard to see the difference between individual particles and grouped clusters in SEM images.

Upon observation, it was discovered that the produced nanofibers had a maximum aspect ratio and a uniform width of 10 to 20 nm. Additionally, it was verified that nanofibers were extracted from the natural chitin of the crab in their native form. Platinum coating was applied to SEM samples prior to analysis. According to Fig. 8, the strong interfibrillar hydrogen connections prevented the nano-chitin powder from fibrillating. Additionally, field emission SEM pictures of the crab shell surface, following the removal of calcium carbonate and proteins, are displayed. SEM pictures revealed chitin nanofibers that were about 10 nm wide. Additionally, wider chitin protein fibres of about 100 nm in diameter were obtained and verified to be bundles of nanofibers with a width of 10 nm.

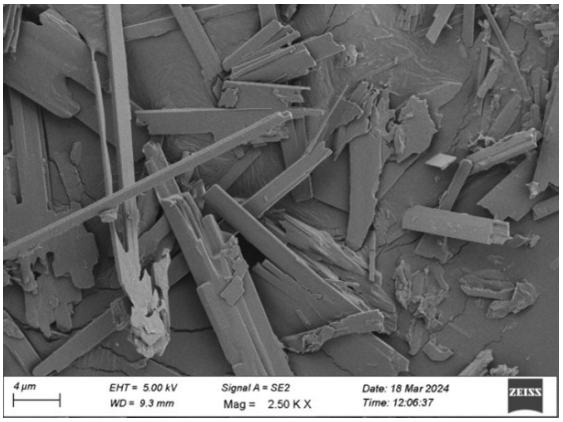

(a)

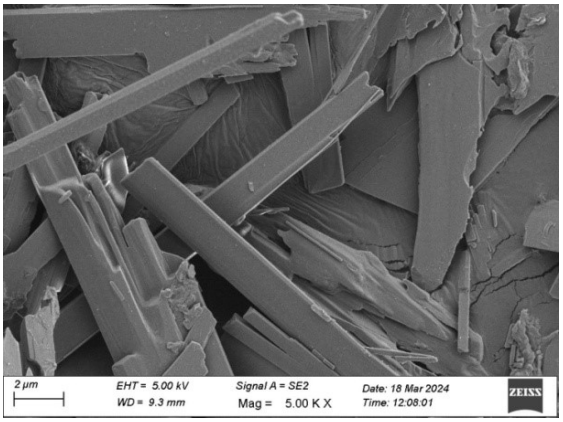

(b)

Fig. 8 SEM micrographs of chitin nanofibers from crab shells. The lengths of the scale bars are (a) 4 µm and (b) 2 µm.

In general, the endocuticle of a crab shell has a bigger fibre diameter and much coarser matrix structure, whereas the exocuticle has a very fine twisted plywood-like structure. The endocuticle typically makes approximately 89% of the crab shell, and because of the wider fibre diameter, it is challenging to fibrillate crab shells. The SEM analysis revealed that the chitin nanofibrils (nano-chitin particles) possess a distinctive morphology, characterized by highly oriented nanocrystals dispersed within an amorphous matrix, along with a relatively uniform size distribution.

The average width was approximately 55.5 nm, indicating the successful nano-structuring of the chitin material. Furthermore, high-resolution imaging of the nano-chitin surface revealed the presence of nanopores and surface irregularities. These nanopores are expected to have a major impact on enhancing the surface area and reactivity of the nano-chitin, making it potentially applicable to a wide range of uses such as water holding capacity, regulated release of nutrients, etc. The SEM analysis also provided qualitative information regarding the purity and homogeneity of the nano-chitin samples. Overall, the SEM analysis confirmed the successful synthesis of nano-chitin with desirable morphological characteristics and surface properties [58].

3.5 SEM analysis of hydrogel

Due to its unique capacity to quickly provide accurate, comprehensive information about morphology, porous topology, cross-linking state, homogeneity, size, shape, and other factors, SEM emerged as the preferred method for morphological evaluation of hydrogels. Three separate samples that had been prepared using the same condition were taken for SEM imaging. When it comes to the pores, integrity, organization, quality, and homogeneity of such materials, its utility is unmatched. Nano-chitin provided a robust support for the hydrogel pore walls according to SEM analysis and enhanced the ability of the hydrogel to absorb water. This caused the pores to enlarge, resulting in a more relaxed and open structure. The three-dimensional porous structure features distinct, linked micropores. SEM analysis revealed that increasing the amount of nano-chitin incorporated into the hydrogel membrane promotes the formation of an interconnected structure. Nano-chitin propensity to absorb water and cause a liquid–liquid phase separation was the cause of this morphological development. Scanning electron microscopy reveals the asymmetric network morphology of the freeze-dried chitin gel, as depicted in Figs. 9(a) and 9(b). The images display the sectional morphology, highlighting the evident chitin hydrogel network, attributed mainly to the increased continuous networks formed by the entanglements as the temperature rises. The preceding SEM micrograph illustrates an asymmetric porous structure, with smaller pore sizes on the surface compared to the bulk. Additionally, Fig. 9(b) provides a clear depiction of the compact and smooth microstructure of the chitin gel surface [59].

The shape recovery characteristics and great flexibility of the nano-chitin hydrogels were demonstrated. After being submerged in water for a few seconds, the hydrogels made from a diluted nano-chitin suspension (0.2 wt%) and squeezed to the utmost extent regained their former shape. Suspensions of 0.1 wt% nano-chitin form weak hydrogels. The grade of the chitin–chitosan hydrogel was determined, with values corresponding to 0.20 g and 0.25 g of water absorbed per gram of gel, respectively. Controlling the cross-linking density, polymer hydrophilicity, recognition entity type, and polymer elasticity allows for the design of the hydrogel characteristics. SEM is an efficient tool for characterizing the morphology of hydrogels in their swollen condition.

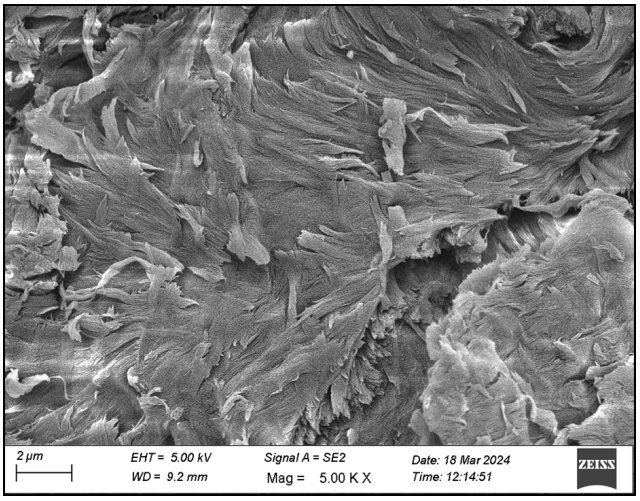

(a)

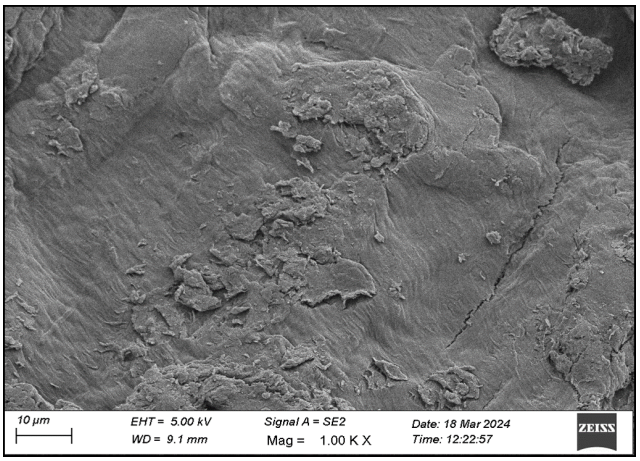

(b)

Fig. 9 SEM of hydrogel (a) section and (b) surface

By using threshold filters and particle analysis functions on the SEM images, the mean and standard deviation of the average diameter of the pores in the hydrogel were determined. It is evident from the SEM pictures that the fibre thickness was comparable to that of nanofibers made from prawn shells that had been broken down in acidic water. After applying a one-time grinding treatment, the twisted plywood structure appears to have crumbled. As a result, although the protein layers were removed without drying, the 100 nm thick fibers were separated from the chitin–protein layers through grinding. This hydrogel that was produced with a single grinder treatment indicates that the nano-fibrillation was successful due to the high surface to volume ratio and strong dispersion property of the nanofiber in acidic water. Highly homogeneous nanofibers of 10 nm width were seen to develop from the disintegrating chitin, indicating that the acidic water promoted the fibrillation process.

The hydrogel developed in this study exhibits promising characteristics for enhanced water retention and precise release of fertilizer, as elucidated by the comprehensive analysis of gel formation and SEM analysis. Through SEM analysis, the intricate network structure of the hydrogel is revealed, showcasing its high porosity and interconnected pores, which facilitate efficient water absorption and retention. Furthermore, the SEM images also highlight pores within the hydrogel matrix, indicating its potential as a carrier for controlled nutrient release. By entrapping the fertilizer within its porous structure, the hydrogel offers a mechanism for gradual nutrient delivery to plants, promoting sustained growth and maximizing nutrient utilization efficiency [60].

3.6 Soil test parameters

The soil test parameters were determined after the hydrogel was inserted into the agricultural plot, and the results are given in Table 4.

4 Applications of hydrogel

The applications of nano-based chitin hydrogels are multifaceted and far-reaching. In agriculture, these hydrogels have been shown to enhance soil waterholding capacity, reduce irrigation frequency, and promote crop growth as shown in Figs. 10(a) and 10(b). Importantly, the hydrogels exhibit biodegradable properties breaking down in the soil without any deleterious side effects, thus offering long term environmental sustainability. Additionally, they can be utilized as seed coatings, providing essential nutrients and water to seeds, thereby facilitating healthy germination and growth. The experiment of plant growth (green gram, *Vigna radiata*) was carried out by using five biological replicates. The mean growth measures were observed. Soil remediation is another area

Table 4 Soil test parameters after nano-chitin hydrogel application

S. No.	Parameters	Unit	Test method	Results
1	Water content	%	IS 2720-2 [32]	12.6
2	Available phosphorous	µg/g	SOP No. Soil/001 [37]	21
3	Ammoniacal nitrogen	mg/kg	IS 14684:1999 [45]	7.4
4	Total Kjeldahl nitrogen	%	IS 14684:1999 [45]	12.6
5	Water holding capacity	%	SOP No. Soil/011 [46]	39
6	Soluble sodium	mg/kg	FAO method [50]	1946
7	Soluble potassium	mg/kg	FAO method [51]	104

(a) (b)

Fig. 10 (a) Growth without hydrogel, (b) growth with hydrogel

where nano-chitin hydrogels can be employed, as they can remove pollutants and improve soil fertility. Table 5 provides a comparative evaluation of chitin-based hydrogels with present study.

In the biomedical field, nano-chitin hydrogels have been explored for their potential in tissue regeneration and pharmacological delivery. Their ability to support tissue regeneration and wound closure makes them an attractive option for wound dressings. Furthermore, these hydrogels can serve as frameworks for tissue engineering, promoting cell growth and differentiation. Their optimized release of drugs also renders them suitable for drug delivery systems. The environmental and industrial applications of nano-chitin hydrogels are equally promising. They can be utilized for water purification, oil spill cleanup, and bioremediation. Moreover, these hydrogels have potential applications in cosmetics, food packaging, and biotechnology, offering a sustainable and versatile solution for various industries [61].

5 Conclusions

Biopolymeric hydrogels, especially those derived from chitosan, have wide-ranging applications, with agriculture being a primary focus. These hydrogels function as water reservoirs and controlled-release agents for nutrients and pesticides, significantly improving soil water retention and nutrient delivery. Chitosan-based hydrogels, in particular, enhance soil conditioning and support sustainable irrigation strategies, thereby influencing crop growth, yield, and survival.

Nano-chitin hydrogels offer additional advantages, including improved seed germination, root and stem development, and nutrient uptake. Their slow-release properties, such as nano-chitin-coated urea, optimize nitrogen

Table 5 Comparative evaluation of chitin-based hydrogels with the present study

Material name	Water holding capacity (%)	Nutrient release efficiency (%)	Biodegradability (days)	Special features/outcomes	Reference
Chitosan-based superabsorbent hydrogel	27	72	15	High elongation at break (2203.7%)	[14]
Starch-based biodegradable hydrogel	30	76	15	High swelling at alkaline pH	[15]
Nano-chitin hydrogel (prior studies)	39	82	15	Tunable mechanical strength, swelling capacity >540%	[16]
Nanocellulose/wood ash-reinforced starch–chitosan	20	65	15	Enhanced swelling (420%), mechanical strength	[26]
Present nano-chitin hydrogel (this study)	50	88	15	Enhanced porosity, 3D structure, sustained urea release	-

use, minimize fertilizer loss, and mitigate environmental impacts. Moreover, these hydrogels can enhance soil structure and microbial activity in areas affected by textile effluents, reducing industrial pollution.

Characterization techniques like FTIR, SEM, and XRD confirm the structural integrity and functionality of the hydrogel. FTIR revealed a new peak at 1631 cm^{-1} and imine bond peaks at 3257 cm^{-1}, indicating successful cross-linking of chitin nanofibrils. SEM analysis validated the morphological homogeneity and purity of the samples, while XRD patterns confirmed the structural changes due to conditioning, especially in water-absorbed gels.

In a controlled study, nano-chitin hydrogels significantly enhanced the growth of *Vigna radiata* (green gram), a globally consumed legume rich in protein. Treated seeds exhibited substantial growth, whereas untreated controls showed minimal development. The non-toxic, biodegradable, biocompatible, and cost-effective nature of hydrogels positions them as promising materials for sustainable agriculture. This research underscores the potential of nano-chitin-based hydrogels to address critical challenges in crop productivity, resource conservation, and environmental sustainability, with far-reaching implications for global food security.

Reflectively, such nano-chitin hydrogel formulation has a scalable future in regard to its synthesis at a pilot level and long-term field test. The upscaling will need the optimization of extraction and cross-linking methods, so that they are consistent in the mechanical and functional performance. Further, it may be combined with intelligent irrigation systems and biodegradable nutrient transporters to make it work better in large-scale sustainable farming. This paves a bright way to commercial potential and general Use in drought-stressed or resource-deficit areas.

References

[1] Jiang, X., Zeng, F., Zhang, L., Yu, A., Lu, A. "Engineered Injectable Cell-Laden Chitin/Chitosan Hydrogel with Adhesion and Biodegradability for Calvarial Defect Regeneration", ACS Applied Materials & Interfaces, 15(17), pp. 20761–20773, 2023. https://doi.org/10.1021/acsami.3c02108

[2] Prasathkumar, M., Dhrisya, C., Lin, F. H., Sadhasivam, S. "The Design and Developments of Protein-Polysaccharide Biomaterials for Corneal Tissue Engineering", Advanced Materials Technologies, 8(15), 2300171, 2023. https://doi.org/10.1002/admt.202300171

[3] Ye, L., Lv, W., He, W., Li, S., Min, Z., …, Xin, H. "Reduced malignant glioblastoma recurrence post-resection through the anti-CD47 antibody and Temozolomide co-embedded *in-situ* hydrogel system", Journal of Controlled Release, 359, pp. 224–233, 2023. https://doi.org/10.1016/j.jconrel.2023.05.046

[4] Dar, S. A., Abd Al Galil, F. M. "Biodegradation, Biosynthesis, Isolation, and Applications of Chitin and Chitosan", In: Ali, G. A. M., Makhlouf, A. S. H. (eds.) Handbook of Biodegradable Materials, Springer Cham, 2023, pp 677–717. ISBN 978-3-031-09710-2 https://doi.org/10.1007/978-3-031-09710-2_72

[5] Zhang, J., Hu, Y., Zhang, L., Zhou, J., Lu, A. "Transparent, Ultra-Stretching, Tough, Adhesive Carboxyethyl Chitin/Polyacrylamide Hydrogel Toward High-Performance Soft Electronics", Nano-Micro Letters, 15(1), 8, 2023. https://doi.org/10.1007/s40820-022-00980-9

[6] Kasprzak, D., Liu, J. "Chitin and cellulose as constituents of efficient, sustainable, and flexible zinc-ion hybrid supercapacitors", Sustainable Materials and Technologies, 38, e00726, 2023. https://doi.org/10.1016/j.susmat.2023.e00726

[7] Taheriazam, A., Entezari, M., Firouz, Z. M., Hajimazdarany, S., Heydargoy, M. H., ..., Sun, D. "Eco-friendly chitosan-based nanostructures in diabetes mellitus therapy: Promising bioplatforms with versatile therapeutic perspectives", Environmental Research, 228, 115912, 2023. https://doi.org/10.1016/j.envres.2023.115912

[8] Meiers, D. T., Rothammer, M., Maier, M., Zollfrank, C., von Freymann, G. "Utilizing the Sensitization Effect for Direct Laser Writing in a Novel Photoresist Based on the Chitin Monomer N-acetyl-D-glucosamine", Advanced Engineering Materials, 25(11), 2201688, 2023. https://doi.org/10.1002/adem.202201688

[9] Ali, M., Mir, S., Abid, O. U. R., Ajlouni, A. W., Ghafoor Alvi, S., Bibi, S. "Applications Of Chitosan Based Bionanocomposites In Drug-Delivery And Anticancer Treatment-A Review", European Polymer Journal, 201, 112576, 2023. https://doi.org/10.1016/j.eurpolymj.2023.112576

[10] Knight, B. M., Edgar, K. J., De Yoreo, J. J., Dove, P. M. "Chitosan as a Canvas for Studies of Macromolecular Controls on $CaCO_3$ Biological Crystallization", Biomacromolecules, 24(3), pp. 1078–1102, 2023. https://doi.org/10.1021/acs.biomac.2c01394

[11] Ruiz, D., Michel, V. F., Niederberger, M., Lizundia, E. "Chitin Nanofibrils from Fungi for Hierarchical Gel Polymer Electrolytes for Transient Zinc-Ion Batteries with Stable Zn Electrodeposition", Small, 19(45), 2303394, 2023. https://doi.org/10.1002/smll.202303394

[12] Escárcega Olivares, F. T., Olayo-Valles, R., García-Arrazola, R., Vázquez-Torres, H., Becerril, E. R., Esparza-Schulz, J. M., Shirai, K. "Valorization of cactus cladode wastes and chitin nanowhiskers in biocomposite designed for sorption of new methylene blue", International Journal of Environmental Science and Technology, 20(12), pp. 13655–13672, 2023. https://doi.org/10.1007/s13762-023-04944-3

[13] Virmani, T., Kumar, G., Sharma, A., Pathak, K., Akhtar, S., Afzal, O., Altamimi, A. S. A. "Amelioration of Cancer Employing Chitosan, Its Derivatives, and Chitosan-Based Nanoparticles: Recent Updates", Polymers, 15(13), 2928, 2023. https://doi.org/10.3390/polym15132928

[14] Dubashynskaya, N. V., Petrova, V. A., Sgibnev, A. V., Elokhovskiy, V. Y., Cherkasova, Y. I., Skorik, Y. A. "Carrageenan/Chitin Nanowhiskers Cryogels for Vaginal Delivery of Metronidazole", Polymers, 15(10), 2362, 2023. https://doi.org/10.3390/polym15102362

[15] López-Saucedo, F., Buendía-González, L., Magaña, H., Flores-Rojas, G. G., Bucio, E. "Crosslinked Chitosan Films Supplemented with Randia sp. Fruit Extract", Polymers, 15(12), 2724, 2023. https://doi.org/10.3390/polym15122724

[16] Sukhavattanakul, P., Pisitsak, P., Ummartyotin, S., Narain, R. "Polysaccharides for Medical Technology: Properties and Applications", Macromolecular Bioscience, 23(2), 2200372, 2023. https://doi.org/10.1002/mabi.202200372

[17] Huang, L. Han, X., Mo, Q., Wang, Y., Wang, X., Li, Y., Huang, C., Duan, Q. "Preparation and properties of modified cassava starch slow-release hydrogel with acid and alkali resistance", Industrial Crops and Products, 206, 117699, 2023. https://doi.org/10.1016/j.indcrop.2023.117699

[18] Almajidi, Y. Q., Gupta, J., Sheri, F. S., Zabibah, R. S., Faisal, A., …, Farhood, B. "Advances in chitosan-based hydrogels for pharmaceutical and biomedical applications: A comprehensive review", International Journal of Biological Macromolecules, 253, 127278, 2023. https://doi.org/10.1016/j.ijbiomac.2023.127278

[19] Azam, A., Ziafat, S. ., Fahid, A. ul M. ., Anjum, F., Faseeh, H., Bano, R., ur Rehman, A., Bashir, A. "Application of Chitosan-Based Polysaccharide Biomaterials in Tissue Engineering", Pakistan Journal of Health Sciences, 4(9), pp. 10–16, 2023. https://doi.org/10.54393/pjhs.v4i09.1038

[20] Luo, G., Xu, Z., Zhong, H., Shao, H., Liao, H., Liu, N., Jiang, X., Zhang, Y., Ji, X. "Biodegradable photothermal thermosensitive hydrogels treat osteosarcoma by reprogramming macrophages", Biomaterials Science, 11(8), pp. 2818–2827, 2023. https://doi.org/10.1039/d2bm01900k

[21] Wan, L., Yan, S., Fang, L., Wang, Z., Zhang, Y. "Liquefied-chitin polyurethane foam construction of high-efficiency solar evaporator for seawater purification", Journal of Applied Polymer Science, 140(21), e53879, 2023. https://doi.org/10.1002/app.53879

[22] Lomartire, S. Gonçalves, A. M. M. "Algal Phycocolloids: Bioactivities and Pharmaceutical Applications", Marine Drugs, 21(7), 384, 2023. https://doi.org/10.3390/md21070384

[23] Elangwe, C. N., Morozkina, S. N., Olekhnovich, R. O., Polyakova, V. O., Krasichkov, A., Yablonskiy, P. K., Uspenskaya, M. V. "Pullulan-Based Hydrogels in Wound Healing and Skin Tissue Engineering Applications: A Review", International Journal of Molecular Science, 24(5), 4962, 2023. https://doi.org/10.3390/ijms24054962

[24] Rani Sethy, T., Biswal, T., Kumar Sahoo, P. "An indigenous tool for the adsorption of rare earth metal ions from the spent magnet e-waste: An eco-friendly chitosan biopolymer nanocomposite hydrogel", Separation and Purification Technology, 309, 122935, 2023. https://doi.org/10.1016/j.seppur.2022.122935

[25] Petroni, S., Tagliaro, I., Antonini, C., D'Arienzo, M., Orsini, S. A., Mano, J. F., Brancato, V., Borges, J., Cipolla, L. "Chitosan-Based Biomaterials: Insights into Chemistry, Properties, Devices, and Their Biomedical Applications", Marine Drugs, 21(3), 147, 2023. https://doi.org/10.3390/md21030147

[26] Barleany, D. R., Jayanudin, J., Nasihin, N., Widiawati, M., Yulvianti, M., Sari, D. K., Gunawan, A. "Hydrogel Preparation from Shrimp Shell-Based Chitosan: The Degree of Crosslinking and Swelling Study", ASEAN Journal of Chemical Engineering, 23(1), pp. 28–39, 2023. https://doi.org/10.22146/ajche.73716

[27] Wu, M., Liu, Y., Cong, P., Mao, S., Zou, R., Lv, J., Tian, H., Zhao, Y. "Study of polydopamine-modified β-chitin nanofiber hydrogels for full-thickness wound healing", European Polymer Journal, 183, 111758, 2023. https://doi.org/10.1016/j.eurpolymj.2022.111758

[28] Kim, Y., Zharkinbekov, Z., Raziyeva, K., Tabyldiyeva, L., Berikova, K., Zhumagul, D., Temirkhanova, K., Saparov, A. "Chitosan-Based Biomaterials for Tissue Regeneration", Pharmaceutics, 15(3), 807, 2023. https://doi.org/10.3390/pharmaceutics15030807

[29] Chen, J., Zhu, Z., Chen, J., Luo, Y., Li, L., …, Luo, B. "Photocurable liquid crystal hydrogels with different chargeability and tunable viscoelasticity based on chitin whiskers", Carbohydrate Polymers, 301, 120299, 2023. https://doi.org/10.1016/j.carbpol.2022.120299

[30] Elango, J., Lijnev, A., Zamora-Ledezma, C., Alexis, F., Wu, W., Granero Marín, J. M., Sanchez de Val, J. E. M. "The relationship of rheological properties and the performance of silk fibroin hydrogels in tissue engineering application", Process Biochemistry, 125, pp. 198–211, 2023. https://doi.org/10.1016/j.procbio.2022.12.012

[31] Lu, H. T.., Lin, C., Wang, Y.-J., Hsu, F.-Y., Hsu, J.-T., Tsai, M.-L., Mi, F.-L. "Sequential deacetylation/self-gelling chitin hydrogels and scaffolds functionalized with fucoidan for enhanced BMP-2 loading and sustained release", Carbohydrate Polymers, 315, 121002, 2023. https://doi.org/10.1016/j.carbpol.2023.121002

[32] BIS "IS 2720-2: Methods of test for soils, Part 2: Determination of water content", Bureau of Indian Standards, Manak Bhawan, Old Delhi, India, 1973.

[33] BIS "IS 2720-22: Methods of Test for Soils: Part 22: Determination of Organic Matter (First Revision)", Bureau of Indian Standards, Manak Bhavan, New Delhi, India, 1972.

[34] BIS "IS 2720-26: Method of Test for Soils: Part 26 Determination of pH Value (Second Revision)", Bureau of Indian Standards, Manak Bhavan, New Delhi, India, 1987.

[35] BIS "IS 14767: 2000 – Determination of the Specific Electrical Conductivity of Soils: Method of Test", Bureau of Indian Standards, Manak Bhavan, New Delhi, India, 2000.

[36] EHS360 Labs "SOP No. Soil/010: Standard Operating Procedure for Soil Testing Sulphate", EHS360 Labs, Chennai, India, 2021.

[37] EHS360 Labs "SOP No. Soil/001: Standard Operating Procedure Available Phosphorous", EHS360 Labs, Chennai, India, 2021.

[38] EHS360 Labs "SOP No. Soil/009: Standard Operating Procedure for Soluble calcium and magnesium", EHS360 Labs, Chennai, India, 2021.

[39] EHS360 Labs "SOP No. Soil/008: Standard Operating Procedure for Soluble calcium", EHS360 Labs, Chennai , India, 2021.
[40] EHS360 Labs "SOP No. Soil/005: Standard Operating Procedure for Carbonate", EHS360 Labs, Chennai, India, 2021.
[41] EHS360 Labs "SOP No. Soil/003: Standard Operating Procedure for Bicarbonate", EHS360 Labs, Chennai, India, 2021.
[42] EHS360 Labs "SOP No. Soil/006: Standard Operating Procedure for Chloride", EHS360 Labs, Chennai, India, 2021.
[43] EHS360 Labs "SOP No. Soil/004: Standard Operating Procedure for Bulk density", EHS360 Labs, Chennai, India, 2021.
[44] EHS360 Labs "SOP No. Soil/007: Standard Operating Procedure for Pore space", EHS360 Labs,Chennai, India, 2021.
[45] BIS "IS 14684:1999: Landslide control – Guidelines", Bureau of Indian Standards, Manak Bhawan, New Delhi, India, 1999.
[46] EHS360Labs "SOP No. Soil/011: Standard Operating Procedure for water holding capacity", EHS360 Labs, Chennai, India, 2021.
[47] EHS360Labs "Standard Operating Procedure for FAO Method for soil texture", EHS360Labs, Chennai, India , 2021.
[48] EHS360Labs "Standard Operating Procedure for Robinson Pipette Method for sand, slit, clay", EHS360Labs, Chennai, India, 2021.
[49] EHS360Labs "Standard Operating Procedure for Inhouse method for Chemical oxygen demand”", EHS360Labs, Chennai, India, 2021.
[50] EHS360Labs "Standard Operating Procedure for FAO Method for Soluble sodium", EHS360Labs, Chennai, India, 2021.
[51] EHS360Labs "Standard Operating Procedure for FAO Method for Soluble pottasium", EHS360Labs, Chennai, India, 2021.
[52] EHS360Labs "Standard Operating Procedure for FAO Method for Cation exchange capacity", EHS360Labs, Chennai, India, 2021.
[53] Li, X., Jiang, L., Yan, M., Bi, H., Wang, Q. "Highly stretchable, tough and conductive chitin nanofiber composite hydrogel as a wearable sensor", International Journal of Biological Macromolecules, 242, 124780, 2023. https://doi.org/10.1016/j.ijbiomac.2023.124780
[54] Wang, K., Huang, H., Sheng, J. "Determination of the Mark-Houwink equation parameters and their interrelationship", Journal of Liquid Chromatography & Related Technologies, 21(10), pp. 1457–1470, 1998. https://doi.org/10.1080/10826079808000527
[55] Wagner, H. L. "The Mark-Houwink-Sakurada equation for the viscosity of linear polyethylene", Journal of Physical and Chemical Reference Data, 14(2), pp. 611–617, 1985. https://doi.org/10.1063/1.555751
[56] Kasaai, M. R. "Calculation of Mark–Houwink–Sakurada (MHS) equation viscometric constants for chitosan in any solvent–temperature system using experimental reported viscometric constants data", Carbohydrate Polymers, 68(3), pp. 477–488, 2007. https://doi.org/10.1016/j.carbpol.2006.11.006
[57] Wan, H., Chen, Y., Tao, Y., Chen, P., Wang, S., Jiang, X., Lu, A. "MXene-Mediated Cellulose Conductive Hydrogel with Ultrastretchability and Self-Healing Ability", ACS Nano, 17(20), pp. 20699–20710, 2023. https://doi.org/10.1021/acsnano.3c08859
[58] Wang, Y., Wang, L., Lu, Y., Zhang, Q., Fang, Y., Xu, D., Cai, J. "Stretchable, Biodegradable Dual Cross-Linked Chitin Hydrogels with High Strength and Toughness and their Potential Applications in Flexible Electronics", ACS Sustainable Chemistry & Engineering, 11(18), pp. 7083–7093, 2023. https://doi.org/10.1021/acssuschemeng.3c00184
[59] Mohite, P., Rahayu, P., Munde, S., Ade, N., Chidrawar, V. R., Singh, S., Jayeoye, T. J., Prajapati, B. G., Bhattacharya, S., Patel, R. J. "Chitosan-Based Hydrogel in the Management of Dermal Infections: A Review", Gels, 9(7), 594, 2023. https://doi.org/10.3390/gels9070594
[60] Liao, J., Wang, Y., Hou, B., Zhang, J., Huang, H. "Nano-chitin reinforced agarose hydrogels: Effects of nano-chitin addition and acidic gas-phase coagulation", Carbohydrate Polymers, 313, 120902, 2023. https://doi.org/10.1016/j.carbpol.2023.120902
[61] Zhatkanbayev, Y., Zhatkanbayeva, Z., Iskakova, Z., Kolpek, A., Serikov, A., Moldagulova, N., Danlybayeva, G., Sarsenova, A., Anuarbekova, S. "Application of Chitosan-Based Hydrogel Obtained from Insects in Pine Planting", International Journal of Biomaterials, 2023(1), 8175405, 2023. https://doi.org/10.1155/2023/8175405